Fracture aperture generation using surface scan measurements of natural rock samples

Brandon Stock[1], **Andrew Frampton**[1,2]

[1]Department of Physical Geography, Stockholm University, Stockholm, Sweden
[2]Bolin Center for Climate Research, Stockholm University, Stockholm, Sweden

Key Points:

- A model for aperture generation based on self-affine theory is improved and evaluated using surface scans of a natural rock sample
- A linear correlation between Hurst exponent and scaling parameter can accurately reproduce the aperture distribution of the natural fracture
- The improved model is shown to successfully generate up-scaled aperture fields using subsections of the natural rock surface

Corresponding author: Brandon Stock, Brandon.Stock@natgeo.su.se

Abstract

In sparsely fractured crystalline rock, aperture variability exhibits significant control of the flow field through the fracture network. However, its inclusion in models is hampered due to a lack of field measurements and adequate numerical representation. A model for aperture generation is developed based on self-affine methods which includes two key parameters, the Hurst exponent and a scaling parameter, and which accounts for relative anisotropy and correlation between the adjacent surfaces forming the fracture. A methodology for analysing and extracting the necessary parameters from 3D surface scans of natural rock fractures is also developed. Analysis of the Hurst exponent and scaling parameter space shows that input combinations following a linear upper bound can be used to generate aperture fields which accurately reproduce measurements. It is also shown that the Hurst and scaling parameters are more sensitive than the correlation between the upper and lower fracture surfaces. The new model can produce an aperture ensemble that closely corresponds with the aperture obtained from the surface scans, and is an improvement on previous methods. The model is also successfully used to up-scale fracture apertures based on measurements restricted to a small sub-section of the sample. Thereby, the aperture fields generated using the model are representative of natural fracture apertures and can be implemented in larger scale fracture network models, allowing for numerical simulations to included representation of aperture internal heterogeneity.

Plain Language Summary

Understanding fluid flow through naturally fractured rock is important for several applications, including subsurface infrastructure and storage of nuclear waste. Many studies assume fractures as smooth planes; however, it is known that real fractures have rough surfaces and a variable aperture, and this variability can significantly control water flow. It is difficult to include an accurate representation of aperture variability in models because of a lack of field measurements, as well as difficulties in creating adequate model-based representations of the variable aperture field. In this study, improvements are made to a previously developed approach for aperture generation, which is based on self-affine theory. The theory is founded on observations of fractal behaviour exhibited by rock surfaces. It is shown that parameter combinations that follow a linear upper bound can be used to generate aperture fields that accurately reproduce the measured apertures. The model is also successfully used to generate up-scaled aperture fields based on a subsection of the fracture sample. Aperture fields generated using this model are representative of natural fracture apertures and can be used in larger scale models, allowing for a realistic representation of aperture variability to be included when simulating flow in models for fractured rock.

1 Introduction

Understanding fluid flow through natural fractured rocks systems is important for several applications, including subsurface infrastructure, storage facilities for spent nuclear fuel and other toxic waste, and hydrocarbon industries (Tsang & Neretnieks, 1998). Flow and transport through sparsely fractured rock is often modelled using a discrete fracture network (DFN) approach because it is well-suited to numerically represent the typically complex geometries observed in fractured bedrock (Cacas et al., 1990; Frampton & Cvetkovic, 2011; Lang et al., 2014). Representation of fractures in DFN models is typically based on the parallel-plate assumption (Witherspoon et al., 1980; Zimmerman & Bodvarsson, 1996), where fracture permeability is often used to represent the aperture void space within fractures. However, DFN models often simplify the effect of internal aperture variability by assuming constant or effectively homogeneous hydraulic properties within the plane of individual fractures. Although most DFN models are able

to numerically include internal variability, its representation is hampered by a lack of field measurements. Also, homogenisation allows for a computationally less demanding description of the fluid flow between fractures, which simplifies run times for large DFNs. Nonetheless, it is well known that fractures are rough walled conduits with varying aperture and multiple contact points (Durham & Bonner, 1994; Novakowski & Lapcevic, 1994; Hakami, 1995; S. R. Brown, 1998), and studies have shown that these features can exhibit control of the flow field through both single fractures (S. Brown, 1987; Nicholl et al., 1999; Zou et al., 2017) as well as fracture networks (Frampton et al., 2019).

Fracture surface roughness has been shown to exhibit self-affine fractal properties (S. Brown, 1987; Power & Tullis, 1991; Renard et al., 2006). Self-affine differ from self-similar fractals as they scale anisotropically along horizontal and vertical reference axes whereas self-similar scale isotropically (Mandelbrot, 1982; Power & Tullis, 1991). The fractal dimension, D, of the surface describes the complexity of the fractal (Malinverno, 1990; Power & Tullis, 1991), and the Hurst exponent, $H = E–D$ (Hurst, 1951), is a measure of the randomness, where E is the number of spatial dimensions in which the fractal is measured. The values of D for rock fractures typically range from 1-1.5 for profiles and 2-2.5 for surfaces (S. Brown, 1987). This agrees with the definition of self-affine fractals where D = 1.5 for profiles compared to self-similar definition where D = 2 (S. Brown, 1987). When describing fracture surfaces using fractals, the Hurst exponent is more convenient (Gallant et al., 1994).

Therefore, in order to generate fractures with internal variability, for example for use in numerical DFN models for flow and transport, the methods used should preserve the self-affine properties of the natural rough-surfaced fractures they aim to reproduce. This includes the Hurst exponent and scaling parameter, but also surface height variability, relative anisotropy, and correlation between the upper and lower surfaces forming the fracture aperture (Ogilvie et al., 2006). Another aspect to take into consideration is the stochastic nature of aperture generation and its needs for numerical DFN modelling. Typically, a large number of fractures are used in models, far more than can realistically be sampled and studied from field investigation. Therefore it is desirable to be able to generate multiple fractures based off of a limited set of fracture aperture measurements, thereby using the same or small set of input parameters to generate multiple fracture realisations (Isakov et al., 2001; Ogilvie et al., 2003). Furthermore, DFN models typically require fractures to be generated at multiple spatial scales, and often at a much greater scale than available from measurements. Thus there is a practical need to upscale fractures, and here, self-affine methods are well suited as spatial rescaling is inherent to their design.

Natural fractures are complex to replicate due to their anisotropy and the correlation exhibited between the upper and lower rough surfaces forming the aperture void space. A root-mean squared (RMS) correlation function has successfully been used to characterise anisotropy on exposed structures (Candela et al., 2009). To obtain variable aperture, two partially correlated rough surfaces are needed. Although generation of independent surfaces is relatively easy, correlation and separation between two surfaces is needed for creating realistic fracture apertures. It is understood that correlation between the surfaces is weak at short wavelengths, where the surface variabilities act reasonably independently of each other, but becomes stronger, and reaches a peak, as wavelength increases (S. Brown, 1987; S. R. Brown & Scholz, 1985; Keller et al., 1999; Ogilvie et al., 2006). Surfaces have been found to be well correlated above the scale of a few millimetres (S. R. Brown & Scholz, 1985; Power & Tullis, 1992).

Several attempts have been made to represent the change in correlation with scale. Previous work by S. R. Brown (1995b) proposed a second surface generated with a 'mismatch length scale'. The wavelengths for the mismatch were obtained from the power spectral density ratio (PSDR). The surfaces are well-correlated at large wavelengths and uncorrelated when the wavelength becomes less than the assigned mismatch length scale.

A set of random numbers can be used to define the phase of the Fourier components which are used to generate the upper and lower surfaces. The correlation between the random number set at different length scales therefore determines the correlation between surfaces of the generated aperture. S. R. Brown (1995b) implemented the uncorrelated length scale by using a second random number generator different from the one used to produce the first surface. This decorrelates the surfaces at scales below the mismatch length, and amplitudes for wavelengths greater than the mismatch length use the same number generator as the one used to create the first surface. This creates a sharp discontinuity between correlated and uncorrelated surfaces. However, Glover et al. (1998b) argued that the transition should be smooth, following a frequency dependent change from high to low correlation. The PSDR function of the surfaces combined with a weighting function was suggested which determines the rate at which the surfaces match with respect to frequency.

Glover et al. (1998b) required two independent random number sets for the wavelengths that are less than the mismatch wavelength, and above this the random numbers are partially correlated. This involved mixing sets of two random numbers using linear weighting. However, Ogilvie et al. (2006) noted that algebraically mixing random number sets in this manner breaks down the distribution produced by the random number generator. Therefore, they proposed an algorithm which swaps the positions of numbers in two random number sets until the desired correlation is reached, producing a partially correlated random number data set. This has the advantage of maintaining the distribution produced by the random number generator as well as enabling the correlation to vary with scale between the two surfaces, producing a more accurate aperture.

Ogilvie et al. (2006) uses several parameters to determine how the matching between surfaces changes with scale based on the PSDR. These are an improvement on previous methods as a minimum and maximum matching fraction can be set and how the change in correlation varies between these two points. However, the overall change from low to high correlation is still a linear change, and even with added parameters to increase the accuracy, it still may not represent natural fractures. That study was also performed on synthetically induced mode I fractures; thus, it is not yet known how well these methods perform when using measurements from and comparing against real-world natural rock fractures.

The aim of this study is to develop and evaluate a method for reproducing rough-surfaced fractures with variable aperture using information obtained from 3D scans of natural rock fracture surfaces. A model for stochastic fracture aperture generation is further developed based on previous work using self-affine fractal concepts, which includes a refined method for representing correlation between the upper and lower surfaces of the fracture. The model is used to generate an ensemble of realisations of fracture apertures, which is evaluated against the measured natural fracture aperture. Furthermore, a detailed sensitivity analysis is conducted on the variability of the Hurst and scaling parameters and the correlation obtained from the surface scans of the fracture in terms of their impact on model performance. Finally, the model is evaluated in terms of spatial up-scaling, where a subsection of the measurements are used to predict the full extent of the fracture.

2 Method

A spectral synthesis approach is used to numerically produce fractals that represent two surfaces which when combined form a fracture with variable aperture void space. A symmetric matrix containing Fourier components is defined, where the Fourier components can be obtained from measurements to obey the various desired properties of the fracture. Each component is comprised of an amplitude and a phase. Fractal dimension and any information about relative anisotropy is contained within the amplitude

component that scales with a power law. Thus, the topography of the fracture surfaces are controlled by the phase of the Fourier components. If the phase is identical for the upper and lower surfaces, the resulting fracture aperture is constant, representing a perfectly mated fracture. In order to create a variable aperture field, the topography of the two surfaces need to be uncorrelated or partially correlated at different wavelengths. When random numbers are used to describe the phase of the Fourier components, the degree of matedness between the surfaces can be controlled by the degree of correlation between the random numbers used.

Natural rock surfaces can be described by a power spectral density function (S. R. Brown, 1995a),

$$G(k) = Ck^{-\alpha} \tag{1}$$

where $k = 2\pi/\lambda$ is the wavenumber, λ is the wavelength which corresponds to distance along the profile, C is a proportionality constant which varies among surfaces and corresponds to the intercept of the logarithm of the power spectrum, and α is the fractal dimension in the range of $2 < \alpha < 3$ which corresponds to the slope of the logarithm of the power spectrum. To obtain the correlation between the upper and lower surfaces of the fracture scans, the power spectral density (PSD) of each surface and the resulting aperture needs to be obtained, which can readily be calculated using Fast Fourier Transforms.

In principle the Fourier decomposition of a surface can be done for an infinite number of wavenumbers k, however in practice there is a clear limit. The limit is defined by the resolution of the surface scans, and any pre-processing interpolation that has been done before calculating the PSD of the fracture surface. When the period of the sine waves are equal to the number of mesh cells in one dimension, then each oscillation of the sine wave exactly covers one cell. Increasing the resolution beyond this point so more sine waves cover a single cell would have no further effect on the amplitude. The maximum frequency that is useful for the surface is therefore $k = 1/N$, where N is the maximum number of cells along one edge length of the fracture scan. When $k = 1$ this corresponds to a sine wave that fits exactly once within the surface.

2.1 Correlation analysis

The correlation of the upper and lower fracture surfaces can be calculated by using the ratio of the PSD from the aperture over the sum of the PSDs of the two surfaces; it is convenient to plot it as a function of wavelength on log-log scale. Ogilvie et al. (2006) called this the PSD Ratio (PSDR, $\xi(k)$), where

$$\xi(k) = \frac{G(k)_{\text{aperture}}}{G(k)_{\text{upper surface}} + G(k)_{\text{lower surface}}} \tag{2}$$

If the PSD ratio tends towards unity for all wavenumbers then the surfaces are completely independent (Glover et al., 1998b, 1998a). If the PSDR is less than unity, then some matching correlation is occurring between the upper and lower fracture surfaces at that specific wavenumber. The correlation at each wavenumber is obtained as $\text{Corr}(k) = 1 - \xi(k)$. Here we introduce a polynomial regression over the PSDR obtained from measurements of a rock fracture from the smallest to largest PSDR(k) value as a convenient approach to remove the fluctuations and get values for the general trend as a function of wavenumber (or wavelength). Fluctuations in the PSDR inevitably occur when calculating the PSD from measurements of fracture surfaces due to natural variability in the upper and lower surface as well as measurement precision.

During aperture generation, different quantities of wavenumbers may be required, and will not necessarily match the amount coming from the measurements of a real fracture. Therefore, the correlation values are typically re-scaled along the length direction of a profile to the correct number of values that are needed for the generation method.

Due to the method of generating a self-affine fractal surface, the dimensions are limited to $2 \times 2^{\mathrm{n}} + 1$ in X and Y, so the correlation values are scaled in length to 2^{n}, which is half of the desired edge length of which the aperture will be generated at. This is important as it will maintain the desired correlation and structure regardless of the resolution used to generate the aperture.

Fractures typically have high correlation at small wavenumbers (large wavelengths), indicating there is large-scale correlation across the fracture. As the wavenumber increases (and wavelength decreases) the matching between the surfaces typically decreases. Once the correlation function $\mathrm{Corr}(k)$ is obtained, a number swapping algorithm is used to create several arrays of different correlation which represent the different wavenumbers. We adopted a method similar to Ogilvie et al. (2006), and developed a number swapping algorithm that swaps the positions of numbers within one random normally distributed array until a set correlation, defined by the matching analysis, is reached between the other random normally distributed array. The algorithm is executed several times such that two correlated arrays are created for every wavenumber that is needed. Correlated pairs of values are selected from the arrays and are placed in two grids that represent the upper and lower surface in the corrected position depending on the wavenumber. This creates a partial correlation between the upper and lower surface that changes with scale. To create different realisations different pairs are randomly selected from the arrays, and the phase of the Fourier components is defined by these random number sets.

2.2 Scaling properties

The other properties needed to generate a self-affine fractal surface are the Hurst exponent H and a scaling parameter. For a self-affine profile to appear similar at different scales, it must be scaled anistropically in two different directions, i.e., length versus topographical height of a rough surface. If the abscissa (length) is scaled by a factor of λ, the ordinate (height) needs to be scaled by λ^H. We adopt the RMS-COR method (Malinverno, 1990; Renard et al., 2006; Candela et al., 2009; Stigsson & Mas Ivars, 2019) to analyse the standard deviation of height difference at different length intervals; at vertices Δv apart the standard deviation σ of the height differences δh is obtained as:

$$\sigma(\delta h(\Delta v)) = \sqrt{\frac{\sum_{v=0}^{N-\Delta v} (h(v+\Delta v) - h(v))^2}{N+1-\Delta v} - \left(\frac{\sum_{v=0}^{N-\Delta v} (h(v+\Delta v) - h(v))}{N+1-\Delta v} \right)^2} \tag{3}$$

where Δv is the number of vertices between the height values being analysed, $h(v)$ is the height value at vertex v, and N is the number of vertices within the line. The Hurst exponent H is obtained by a log-log fit of the standard deviations σ against the distance between the vertices Δv; the slope of the line corresponds to H and the intercept corresponds to the standard deviation of adjacent vertices δh, the value which is used to scale generated surfaces.

The method is relatively easy to implement but affected by the finite length of trace profiles. Therefore, Δv must be small compared to N; for this reason if Δv is above approximately 10% of maximum trace length it is not considered reliable (Marsch & Fernandez-Steeger, 2021). The Hurst exponent can also be underestimated due to the finite trace length. However, the RMS-COR method is considered to under-estimate Hurst exponents when $H > 0.5$ (Stigsson & Mas Ivars, 2019). Therefore, we implement the following correction as suggested by Marsch and Fernandez-Steeger (2021); if $H_{RMS,cal} > 0.5$ then $H_{RMS} = \ln(H_{RMS,cal}) + 1.18$.

2.3 Surface scans of a natural fracture

The rock sample was taken from a medium grained granite block from the Flivik quarry in Oskarshamn municipality, Sweden, and includes a natural vertical fracture running through it. The sample cut from the rock slab was 200 x 200 x 250 mm^3 containing the partially mated fracture. A force of approximately 100 Nm was required to break the remaining rock bridges between the surfaces and open the fracture (Bruines, 2022). Figure 1a shows the fracture surface after opening.

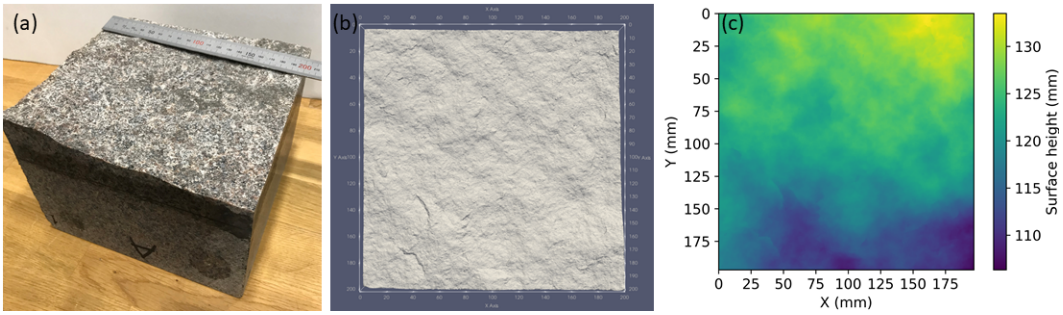

Figure 1. Upper surface of the fracture after opening (a), 3D scan of the surface (b) and surface after interpolation from point cloud data to a regular grid (c).

Once opened, the upper and lower surface were scanned using a handheld laser scanner (Figure 1b). The surface scan data required pre-processing before it could be used to obtain the parameters needed for aperture generation (Stock & Frampton, 2022). The scanning method used results in an irregular mesh. This means on the XY coordinate plane, the nodes on the upper and lower surface will not align. Due to this, the surface data is linearly interpolated onto a regular grid with a resolution of 0.1 mm in order to easily obtain the aperture field (Figure 1c). Areas near the edge of the scan tend to contain errors so the edges are cropped to remove obviously erroneous data. Issues arise from vertical referencing of the upper and lower surface scans, resulting in an unrealistic aperture field with many negative aperture values. To correct this the lower surface is translated relative to the upper surface to improve alignment and reduce inaccurate negative apertures. However, this is insufficient to fully correct the aperture field, so pressure film data that was also provided was used as a reference to vertically shift the upper surface until a visual best fit aperture field distribution is achieved. Further details on pre-processing the surface scan data are presented by Stock and Frampton (2022).

After pre-processing, the surface scans produce an aperture that contains a few abnormal isolated larger apertures, which are most likely due to rock fall out during opening of the fracture. Figure 2 shows the rock fall out collected after opening (a) and the aperture when 5% of the largest apertures have been removed (b). As can be seen, the largest values generally occur in isolated locations across the aperture field. Areas that have a constant value of zero are considered contact points, and areas that are white are where data has been removed (b). An interpretation of the pressure film is also shown (c) with locations of the rock fall out highlighted, white areas represent void spaces that are larger than the thickness of the pressure film (200 μm) and red represents a pressure of 50 MPa.

Figure 3 shows the normalised cumulative distribution and box plots for the same aperture whilst systematically filtering the largest values from the data by area. Zero percent represents the full aperture with no data removed and 5% represents the aperture where the largest 5% of aperture values are removed. During opening the fracture, release of stress could lead to the surface level increasing, which results in a negative aper-

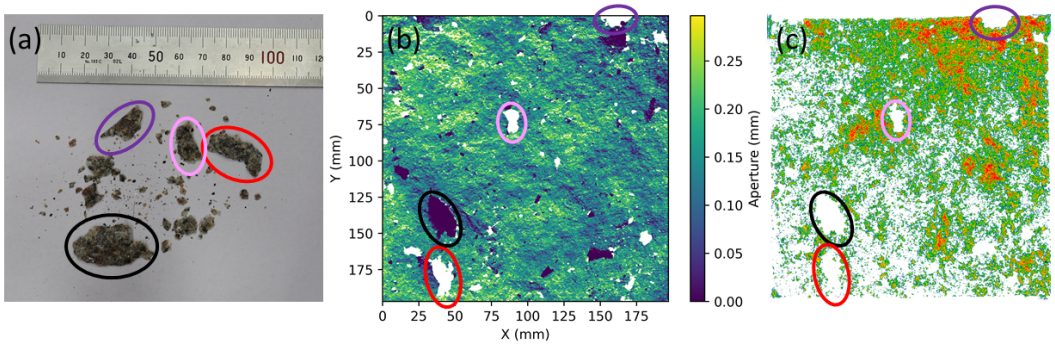

Figure 2. Rock fall out collected after opening the fracture (a) with the possible locations of fall out located on the aperture field by red, black and pink circles (b) and pressure film data (c)

ture when the lower surface is subtracted from the upper surface. Therefore, all negative apertures have been set as zero and are assumed to be contact areas. Removing the largest 1% of apertures significantly reduces the maximum aperture by approximately 2 mm, this highlights how isolated the largest apertures are. As increasingly larger percentages of the aperture are removed, the maximum values decrease whilst only having small changes on the aperture distribution. The change in distribution is mainly observed as the normalised cumulative distribution reaches approximately 0.9, and apertures with a higher percentage of filtering reach the peak sooner. The differences between successive percentage increase of filtering become smaller, with 4% and 5% having only minor differences in distribution. Box plots for the distributions (Figure 3b) show a decrease in most values as larger percentages of the aperture are removed. However, the median value remains fairly constant, decreasing from 0.149 mm at 0% to 0.146 mm at 5% filtering. The consistency in the medians shows that when the whole aperture is considered the largest apertures are outliers within the data set. No outliers are present at 5% filtered, so this aperture is used for comparison with the generated aperture.

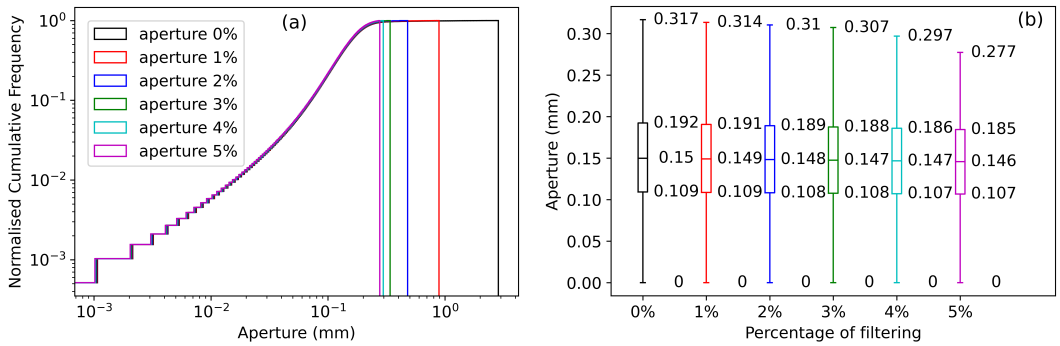

Figure 3. Normalised cumulative distributions of the measured aperture with the maximum apertures filtered by increasing percentages of area (a) and corresponding box plots (b)

2.4 Fracture surface and aperture generation

Several trace profiles are taken across each of the two fracture surfaces (cf. upper, shown in Figure 1c) in the X and Y directions along every mesh cell, so that the total number of profiles in one direction is the same as the total number of cells along one edge

length. This results in 1970 trace profiles in each direction, with a length resolution of each trace profile of 0.1 mm. The RMS-COR method is then executed on every profile, providing a Hurst and scaling parameter for each profile, where a combination of parameters that most closely represents the surface must be selected (section 3.1). Relative anisotropy is calculated by using the median of the ratios $H(X)/H(Y)$. The Hurst exponent and anisotropy are then used to define the amplitude of the Fourier components.

When all the Fourier components are known and arranged in a 2D complex and symmetric matrix in the correct position regarding wavenumber, a 2D Fast Fourier Transformation is executed over the data, the real part of which represents the fracture surface with a mean value of zero. The last steps are to scale the surface to the required size, and scale the asperities to that defined by the scaling parameter obtained from the RMS-COR method, and vertically shift the mean level of the fracture surface such that no negative values occur in the aperture field. It is important to account for different trace resolution between the real data and generated aperture, so the scaling value can be corrected to represent the same resolution, and hence produce an accurate re-scaling of the surface and aperture. Note that the topography of each pair of surfaces will depend on the random number sequence used to select the correlation arrays. Therefore, due to this stochastic nature of sampling, an ensemble of fracture aperture realisations must be generated for a given set of input parameters in order to obtain a sufficiently large sample size to compare against the measured fracture aperture. However, we stress that each generated sample is an equally probably realisation based on a given set of input values. Therefore, this can enable a convenient approach for generating multiple fractures based on a limited number of fracture measurements. Furthermore, since the scaling behaviour of the surface and relative positions of different size asperities is controlled by the Hurst exponent, it enables a convenient approach to up-scaling fracture surfaces, based on the assumption of the properties of the rough surfaces being self-affine for the spatial scales considered and the correlation between surfaces being scale independent.

3 Results

3.1 Fracture surface and aperture field

The PSDR obtained from the fracture with a third order polynomial regression plotted over the PSDR is shown in Figure 4a. The variation in correlation with wavenumber shows the decrease in correlation (Figure 4b, red line) as wavenumber increases. The number of wavenumbers over which the correlation is applied has been re-scaled to correspond with the dimensions at which the aperture realisations will be generated at. As can be seen, the correlation 1 - PSDR (Figure 4b, blue line) initially decreases before increasing again at approximately 50, however the correlation reaches a minimum value of approximately 0.86. The increase thereafter is an artefact due to the resolution of the surface scans and the resolution at which the surfaces were interpolated on to a regular grid. If one value in the point cloud is interpolated over more than one grid cell then 1 - PSDR will increase. This artifact is removed from the correlation array (red line) by manually setting the minimum value for increasing wavenumbers. This adjusted correlation function is then used in the subsequent number swapping algorithm.

The RMS-COR method is then executed on trace profiles across both surfaces in the X and Y directions every 0.1 mm using a maximum step length of 10% (Δv, Eq 3), resulting in 1,970 values of both Hurst exponent and scaling parameter in each direction on the upper and lower surfaces. The 75^{th} percentile for Hurst exponent and scaling parameter have been used to generate the partially correlated upper and lower surfaces and resulting aperture field that are seen in Figure 5. The cumulative density function of the single realisation of the aperture field is shown in Figure 6a. Thereafter, multiple realisations using the same input parameters are generated; the ensemble of 100 realisations are shown in Figure 6b.

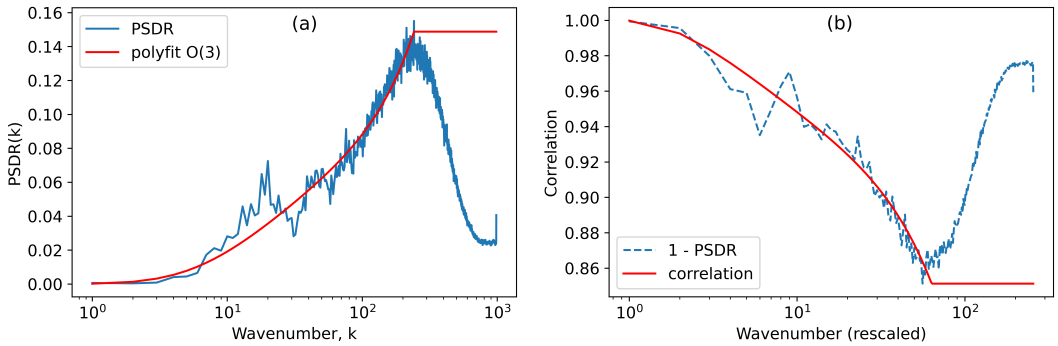

Figure 4. PSDR with a third order polynomial regression (a) and change in correlation with rescaled wavenumbers (b)

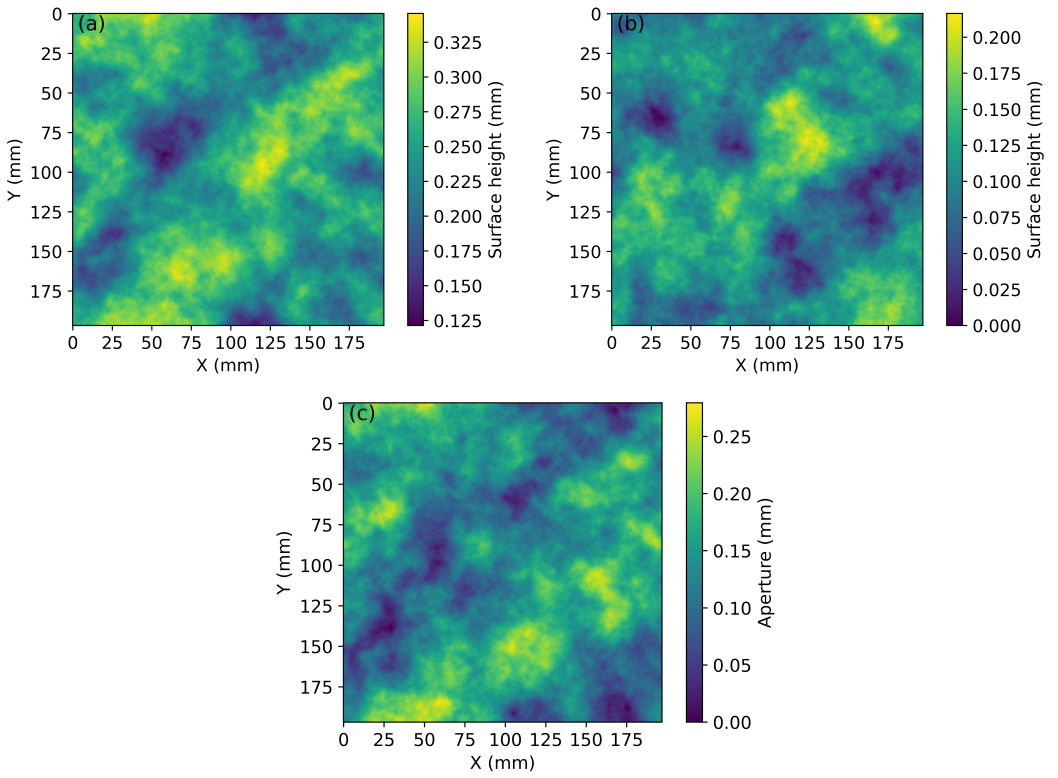

Figure 5. Generated upper surface (a), lower surface (b) and resulting aperture field created from the semi correlated surfaces (c)

The spread in aperture distribution is due to the stochastic nature of the method, therefore multiple realisations are required to be generated until the aperture ensemble stabilises. The number of realisations required is evaluated by using the two-sided Kolmogorov-Smirnov test to compare the measured aperture distribution with increasing generated aperture ensembles (Table 1). A smaller KS value represents a closer match, and a value of 0 indicates the two empirical distributions are identical. This shows that 50 realisations and greater will show very little variation; in the main analysis 100 realisations are used.

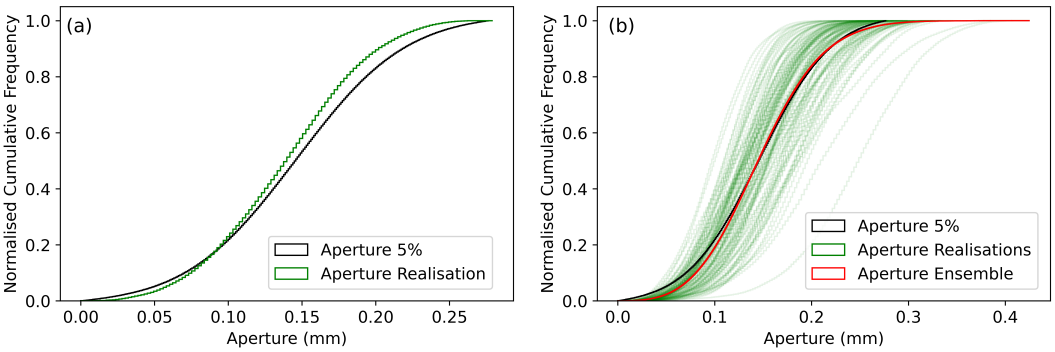

Figure 6. Cumulative distribution of one realisation (a) and a 100 realisations with generated aperture ensemble (b)

Table 1. KS test statistic for ensembles comprised of increasing number of aperture realisations tested against the 5% filtered measured aperture

No. of realisations	KS statistic
10	0.043
20	0.056
50	0.035
100	0.034

There is a significant spread in Hurst and scaling parameters, and which differs slightly between the upper and lower surfaces (Figure 7a,b). The Hurst exponent ranges from approximately 0.6 to 1 for both the upper and lower surface but a larger difference between the surfaces is seen in the scaling parameter, which ranges from 0.025 to 0.06 and 0.025 to 0.07 for the upper and lower surfaces respectively. The 25^{th}, median and 75^{th} percentiles have been calculated for both Hurst exponent and scaling parameter (Table 2). The input parameters from the 75^{th} percentiles generate an aperture ensemble distribution that corresponds well with the measured aperture field scans, better than using the median, and the 25^{th} percentile showing the most dissimilar distribution (Figure 7c). However, note that any of the parameter combinations plotted could be used for aperture generation, so the combination that produces an ensemble most similar to the aperture data must be determined.

3.2 Parameter sensitivity analysis

The analysis of the fracture scans yields a wide range of values for the Hurst exponent and scaling parameter (Figure 7 and Table 2). Here we present an analysis of these parameter combinations in terms of their impact on the resulting generated aperture field distribution. A regular grid of points across the parameter space is considered, which has the advantage of providing a systematic analysis for regions both covered by the pairwise correlated Hurst and scaling parameters as well as regions beyond. Each pair of Hurst exponent and scaling parameter in the grid is used to generate 100 realisations of the aperture field, and the ensemble evaluated against the measured aperture distribution. The similarity of the generated ensembles with the measured aperture was assessed using the Kolmogorov–Smirnov (KS) test statistic, which measures the largest difference between the distributions of the two samples. Figure 8 shows an overlay of the KS statistic value, where a smaller value means a better fit between the distributions, on the reg-

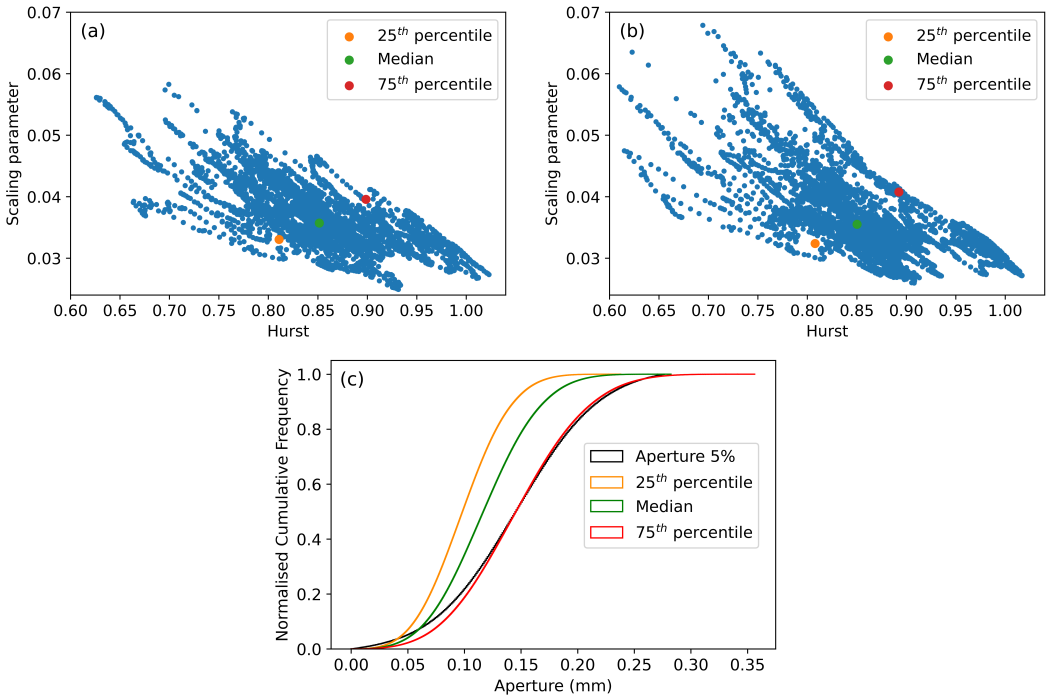

Figure 7. Hurst exponent and scaling parameter from each trace profiles along X and Y directions for the upper (a) and lower (b) surfaces and the corresponding cumulative distribution of the aperture ensembles using the 25th, median and 75th percentiles as input parameters (c)

Table 2. The 25th, median and 75th percentiles for Hurst exponent and scaling parameters for the upper and lower surfaces using different maximum step lengths in the RMS-COR function

Upper surface	Step length 20%		Step length 10%		Step length 5%	
	Hurst	Scaling	Hurst	Scaling	Hurst	Scaling
25th percentile	0.660	0.040	0.811	0.033	0.875	0.030
Median	0.755	0.046	0.851	0.036	0.913	0.032
75th percentile	0.822	0.057	0.899	0.040	0.947	0.034

Lower surface	Step length 20%		Step length 10%		Step length 5%	
	Hurst	Scaling	Hurst	Scaling	Hurst	Scaling
25th percentile	0.653	0.040	0.808	0.032	0.873	0.029
Median	0.747	0.047	0.850	0.036	0.913	0.031
75th percentile	0.817	0.057	0.892	0.041	0.951	0.035

ular grid parameter points over the scatter plots of parameters on the upper and lower surfaces. A linear regression was plotted using the weighted overlay to follow the trend of best fits (Figure 8, black line) which generally follows the upper bound of the parameters. Moving away from this trend results in an increase in the KS statistic value as the

parameter combinations generate apertures that are less similar to the measured aperture. The 75$^{\text{th}}$ percentile combination for the Hurst and scaling parameter is very close to the linear regression line, and the ensemble generated using these values has the smallest KS statistic value. Therefore these values are used as input parameters for the final aperture generations.

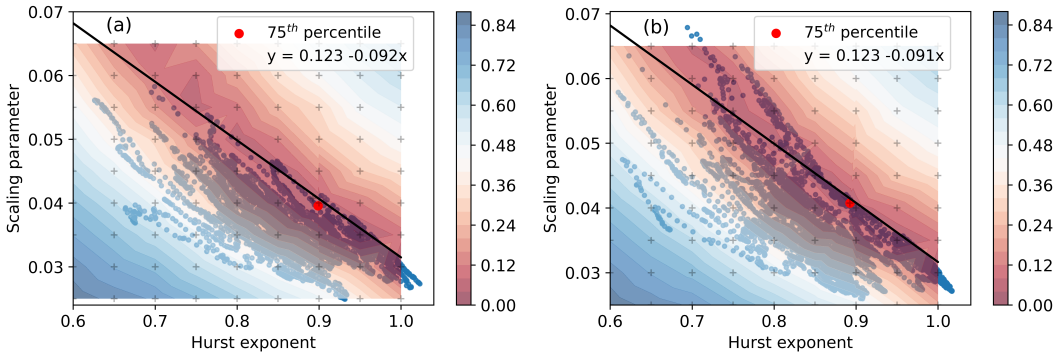

Figure 8. Hurst exponent and scaling parameter scatter plot overlain with fitting metric results for the upper (a) and lower (b) surfaces with the 75$^{\text{th}}$ percentile highlighted and regression line plotted using the weighted overlay

Figure 9a shows the correlation obtained from a polynomial fit which we propose here (red line) compared against the correlation obtained using the approach suggested by Ogilvie et al. (2006) (blue line). It can be seen that our approach has a lower gradient of change from low to high correlation, meaning that at larger wavelengths the surfaces are not as strongly correlated as they would be compared to the approach by Ogilvie et al. (2006). The main difference is that the approach we suggest uses all of the information obtained from the PSDR analysis of the fracture scan sample; it does not solely rely on end points of the correlation and length over which the transition occurs. By introducing the polynomial fit of the PSDR, the generated aperture ensemble distribution is improved and better corresponds with the measured fracture sample (Figure 9b).

Box plots for the filtered aperture show the aperture ensemble generated using the Ogilvie et al. (2006) method and the new model developed in this paper (Figure 9c). This shows that the Ogilvie et al. (2006) method under predicts the distribution, with each of the values being lower than the filtered aperture data. However, the new model has a distribution that is very similar; the median value is only 0.001 mm smaller, with the biggest difference seen in the upper whiskers which are 0.013 mm larger.

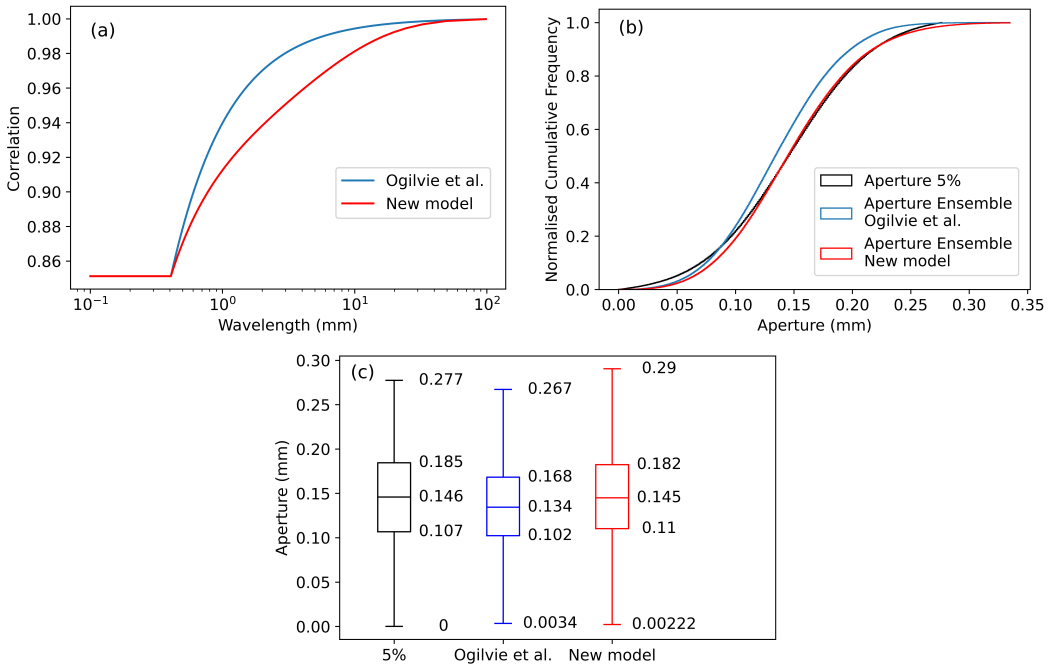

Figure 9. Comparison of Ogilvie method and the new model correlation with wavelength (a), aperture ensemble distribution generated from the new correlation and input parameters (b) and box plots of the 5% filtered aperture, Ogilvie method and new model ensemble (c)

4 Discussion

4.1 Field data filtering

During opening of the fracture some rock was broken off (Figure 2a), and although the volume of this debris is unknown it could be the cause of isolated and abnormally large apertures seen in the unfiltered distribution (cf. Figure 3a). The shape of some of the debris has similar geometry to the larger apertures, which further suggests that rock fall out is the cause. This is highlighted by red, black, purple and pink circles around rock debris and the possible location on the aperture field. The red, purple and pink circle encompass rock pieces that have a distinct shape, which seems to also be present in the aperture field and also in the pressure film data (Figure 2b,c). If the rock debris would have remained intact in these locations, the corresponding apertures would be significantly smaller. However, it is difficult to predict how adding the rock pieces would affect the apertures. For this reason, the aperture data has been filtered to remove the largest 5% of apertures, which should correct for the rock fallout and provide a more accurate representation of the distribution of the aperture when it was unopened. However, excessive filtering increases the risk of unintentional removal of large natural fracture apertures. We determined the threshold limit of 5% to be a reasonable balance without excessively impacting the overall shape of the aperture distribution (cf. Figure 3).

Another piece of rock fallout that visually fits well is highlighted by a black circle. This location represents a contact area, which is due to the subtraction of the lower surface scan from the upper resulting in a negative aperture, hence it is corrected to zero. It is not intuitive how additional rock mass would correct this, however from the pressure film data there is also a large void space at this location. This suggests that the rock piece was loosely attached during scanning, but has fallen off before the pressure film measurements were taken. If the piece was attached then a higher pressure would be ex-

pected, representing close contact, however it can be seen there is a void space at this location (Figure 2, black circle). This highlights further that great care should be taken when using the pressure film to vertically align the surfaces, as the 3D scan data and pressure film may not represent exactly the same state of the surfaces and resulting aperture field.

4.2 Hurst exponent and scaling parameter space

The spread of Hurst exponent and scaling parameter is in part due to the maximum step length that is used when calculating RMS-COR function. Figure 10a,b shows the spread of parameters using a step length of 20%, 10% and 5% (orange, blue and green respectively) of the maximum trace length. Reducing the step length reduces the likelihood of the regression line curving in log-log space, and hence reduces the spread (Marsch & Fernandez-Steeger, 2021). It should be noted that changing the step length has no effect on the total number of Hurst and scaling values as the same number of trace profiles are used. When a maximum step length of 20% is used the spread is large, ranging from approximately 0.35 to over 1 for the Hurst exponent. Small Hurst exponents seen in this range are not likely to be seen on fracture surfaces, as generally the Hurst exponent will range from 0.5 to 1 (S. Brown, 1987). As Hurst exponent decreases, it can be seen that some values of scaling parameter and Hurst exponent create a trend away from the main bulk of the scatter plot. This can most clearly be seen for a maximum step length of 20% at the lower Hurst exponent values. Potentially this could be due to trace profiles that go over sections where substantial parts of rock surface have fallen out during opening, which may perturb the assumption of the fractal nature of the fractures. Reducing the step lengths reduces the spread of these data away from the main bulk of the scatter plot, reducing errors that have been introduced from a larger step length. This reduction also decreases the extent by which the scatter plot data goes above the linear regression that represents a line along which parameter combinations produce the best correspondence between aperture ensemble distributions and the measured aperture.

For the upper surface it is only the data obtained from a maximum step length of 20% that has a significant amount of values above the regression line, with the other two data sets mostly staying below this line. This shows that for the upper surface the best parameter combinations fall on the upper bound of the data. For the lower surface this is not so obvious, as regardless of the step length, some of the parameter combinations fall above the linear regression. The Hurst exponent at which the values go above the linear regression decreases as the maximum step length increases. However for smaller step lengths, the majority of the data points stay below the linear regression line, suggesting the influence of rock fall out is also present in the lower surface. Table 2 shows the affect of maximum trace length on the 25^{th}, median and 75^{th} percentiles for Hurst exponent and scaling parameter.

When the maximum step length of 10% is used, the 75^{th} percentile is on the upper bound of the data for both the upper and lower surface, which also is very close to the regression line that represents the parameter combinations that produce the best aperture ensembles (Figure 10c,d). When the step length is reduced further to 5% then 75^{th} percentile is slightly further away, but would still produce reasonably good aperture ensembles. However, if a larger maximum step length is used then this value moves significantly above the regression line, which is seen for the maximum step length of 20% and would not produce an aperture ensemble that corresponds well with the measured aperture. This shows that a maximum step length of 10% is best when the full surface is used to obtain the 75^{th} percentile parameter combination. This percentile lies on the upper bound of the data and is easy to calculate, making it easy to find this parameter combination as the input. However, any parameter combination along the linear regression line could be used as the input and produce an aperture ensemble that corre-

sponds with the measured aperture. The surfaces will have different topographies, but the resulting aperture distributions will be consistent. The regression line could represent a natural upper limit of the surface roughness, where values along this line best represent that specific surface. Hence, different rock and fracture types with different properties may have a different gradient to the line of regression.

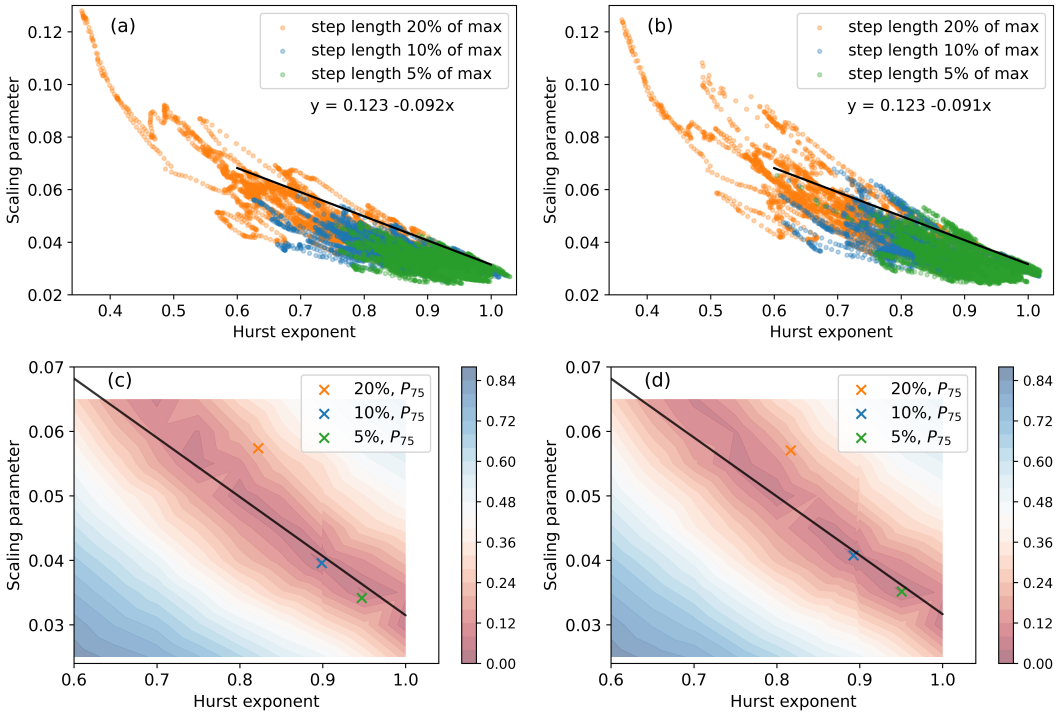

Figure 10. Upper (a) and lower (b) surface Hurst and scaling parameters for 20%, 10% and 5% of the maximum step length and regression line calculated from best fit overlay. The 75th percentiles for a maximum step length of 20%, 10% and 5% for the upper (c) and lower (d) surfaces and the linear regression line following the best fits

The method used to calculate Hurst exponent and scaling parameters used in this study is different from Ogilvie et al. (2006) as they used the slope of power spectral density to obtain these parameters. However, using the power spectral density to obtain input parameters can be affected more greatly by rock fall out which creates areas that are no longer self-affine. When used to calculate the Hurst exponent from these surfaces the result is a value of 0.52, compared to approximately 0.9 which is the 75th percentile value of the method we use. This could have worked for Ogilvie et al. (2006) as the fractures used in that study were artificially induced, therefore there was not the issue of forcing the fracture open and damaging the surfaces in the process to produce rock fall out. Since the fracture in this study is natural, using many traces across the surface and the RMS-COR evaluation method works better. This also allows the values which are most representative of the surface to be selected, as well as allowing the scaling parameter to be obtained from the same method.

This method can also work on fracture trace profiles, if the full surface is not available for analysis. The correlation can be obtained from this data, but only one set of parameter combinations will be obtained, meaning the 75th percentile is unknown. In this case a maximum step length of 5% is best, as the spread of data is reduced (Figure 10a,b),

so it more likely that the Hurst and scaling parameter will be close to the best fit regression line.

4.3 Upper and lower surface correlation

The model for aperture generation presented in this work has updated the method in which the correlation with scale changes. The PSDR is used, as it is in Ogilvie et al. (2006), but each wavenumber is used, which avoids the need to calculate a linear change between minimum and maximum correlation between the surfaces. Instead we can plot a polynomial regression through the PSDR (Figure 4) and base the correlation for each wavenumber off this, giving a more realistic transition from low to high correlation between the surfaces as the scale changes. Depending on the order of polynomial however, it might not capture all the fluctuations. For example, as the correlation decreases with increasing wavenumber (decreasing scale) there are small fluctuations around wavenumber 9 (Figure 4). The fluctuations could be a result of large isolated apertures, as this wavenumber is approximately equivalent to the distance between large apertures, and could lead to the spike in the power spectral density that is observed. This fluctuation is not however captured in the correlation if a low order polynomial is used.

A sensitivity analysis of the aperture generation model to correlation with scale was tested using several different order polynomial regression fits. As can be seen from Figure 11a,b using order 3, 9 and 16 has very little effect on the overall distribution. This suggests that it is the general trend that is more important to capture than every small fluctuation. The general trend captured from a third order polynomial regression is different from the linear change that has been implemented in previous methods, and the improvements can be seen in Figure 9 where the update to correlation produces a generated aperture ensemble distribution that highly corresponds with the measured aperture field.

Also, a synthetic analysis was conducted over an arbitrarily selected correlation with scale, but one that could be expected within reality (Figure 11c). Ten cases, each with a 100 fracture aperture realisations were systematically generated, with initially only wavenumber 1 correlated to the maximum value, increasing until the first 10 wavenumbers have a constant high correlation. After this point there is a decrease in correlation as the wavenumbers increase as would be expected in a natural fracture. Distributions created with wavenumbers 2 to 10 highly correlated are grouped together, and show no systematic change as the wavenumbers increase (Figure 11d). However when only wavenumber 1 is highly correlated, it is clearly separate from the other distributions. This suggests that correlating the first wavenumber correctly is more important than the following wavenumbers as the scale increases. Using a low order polynomial regression allows the first wavenumber to be accurately obtained while plotting the general trend of correlation for the following wavenumbers, allowing an accurate representation of the aperture field to be produced.

Although the large apertures have been filtered out when comparing the realisations to the measured aperture, they are still present when calculating the PSDR and the correlation with scale. This may lead to slightly inaccurate correlation within the generated apertures. This could be corrected for if a reliable method for correcting surface scans is produced. However, currently there is no way to accurately digitally replace any rock fall out. To remove these areas during the matching analysis would also produce errors with the correlation, most likely to an even greater extent. Errors from the matching analysis are a direct consequence of fall out during opening the fracture and scanning. Therefore it is imperative that this process be done as accurately as possible to allow for more accurate realisations of the aperture to be generated.

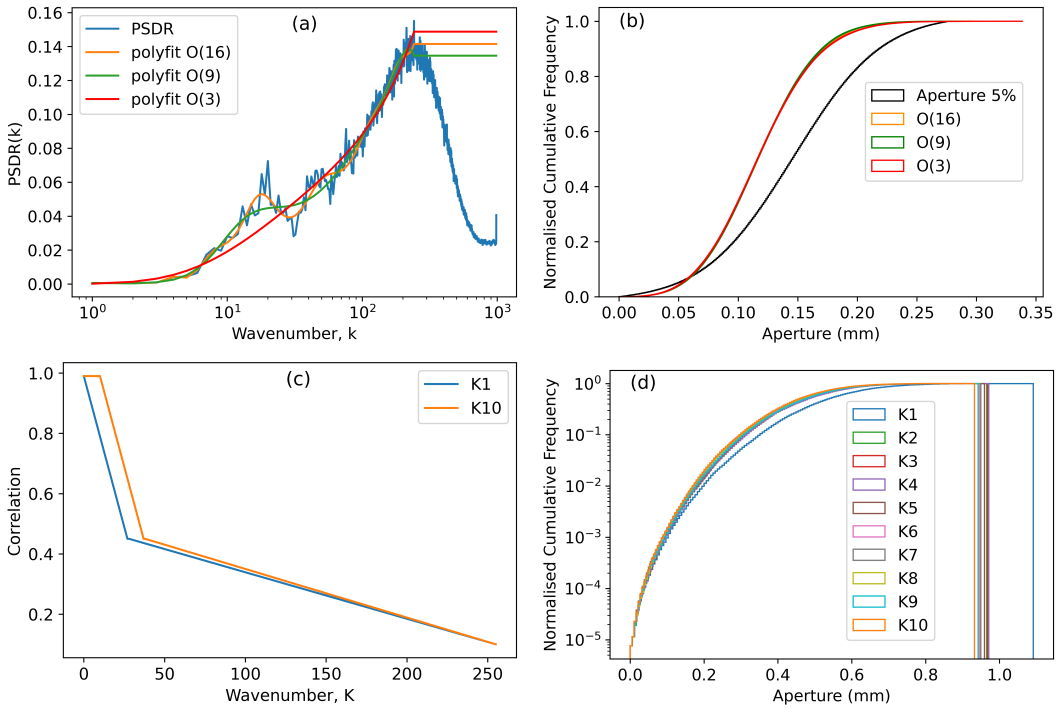

Figure 11. PSDR with different orders polynomial regression fits (a) and the resulting aperture distribution ensembles (b). Change in correlation with wavenumber for cases with the first wavenumber, K1, and the first 10 wavenumbers, K10, highly correlated (c) and the effects of increasing the amount of wavenumbers (K) that have the highest correlation on the aperture ensemble (d)

4.4 Implications for up-scaling

One reason for developing this method is to allow for representations of real fracture apertures to be up-scaled and implemented within larger scale DFNs. Figure 12a,b shows a scatter plot of Hurst exponent and scaling parameter for the full surface and a 100 mm^2 subsection. The linear regression represents the line along which the parameter combinations show the best correspondence with the measured aperture. As can be seen the 75$^{\text{th}}$ percentiles are situated close to the linear regression for parameters obtained from both sized sections, where blue represents the subsection and orange represents the full surface. For up-scaling the Hurst and scaling parameter should be selected from the upper bound of the data, and not a single value. The cropped section of the full surfaces has been used to generate an ensemble of 100 aperture realisations which have been up-scaled to 197 x 197 mm^2, the results of which can be seen in Figure 12c,d. The difference between the median is 0.01 mm for the full aperture and 0.006 mm for the cropped aperture field. When the matching analysis is undertaken on the subsection, the correlation between the surfaces is slightly weaker, resulting in larger apertures when the up-scaled apertures are generated, leading to the difference in medians. However, overall the difference is only small and the ensemble corresponds moderately well with the measured aperture data, showing that this method can be used to up-scale aperture fields to any desired dimensions. Although this method does allow for up-scaling based solely on a fracture trace profile, it will not be as accurate as using a surface scan of the fracture surfaces.

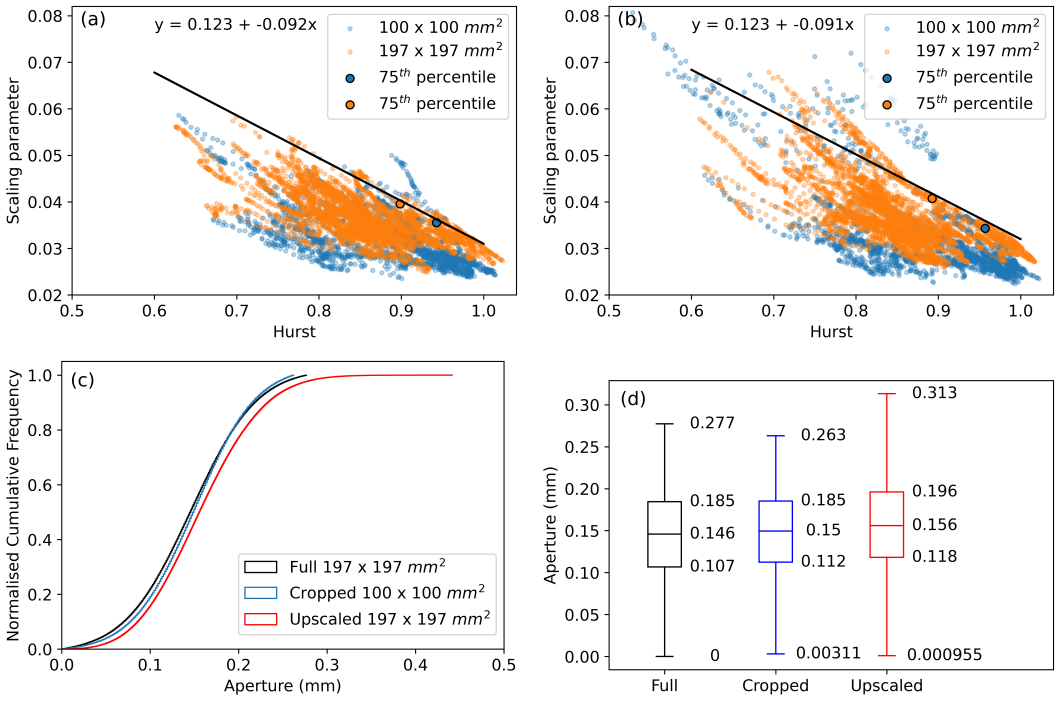

Figure 12. Hurst exponent and scaling parameter for the upper (a) and lower (b) surfaces with different dimensions, cumulative frequency of the full aperture, cropped and up-scaled aperture ensemble (c) and resulting box plots (d).

5 Conclusion

The method developed in this study can generate apertures that are representative of natural rock fractures based on data from high resolution 3D fracture surface scans. During opening of the fracture, rock debris fell out, resulting in abnormally large apertures in the measured aperture distribution, which required filtering before comparison. The generated aperture ensemble distribution shows very high correspondence with the filtered measured aperture distribution. The approach to obtaining a correlation between upper and lower fracture surfaces has been improved based on previous methods by using a third order polynomial regression. This results in a general trend of change in correlation with scale which is implemented over the required wavenumbers. The changes in the minimum correlation at high wavenumbers can slightly affect the aperture distribution which can be seen from the up-scaled aperture realisations.

However it was found that fluctuations in correlation between the surfaces is not as sensitive as the input parameters that are used. The Hurst and scaling parameter are shown to exhibit a clear linear correlation, visible when plotted on a scatter plot; as the Hurst exponent increases the scaling parameter decreases. Reducing the maximum step length in the analysis of profile traces along the fracture surfaces reduces the spread of data and the number of outliers deviating away from the main trend.

Also, we show that using the 75^{th} percentiles for the Hurst exponent and the scaling parameter result in aperture distributions that correspond very well with the measured data. It was found that any parameter combination along a linear regression which follows the upper bound of correlation between the Hurst and scaling parameters would result in an aperture ensemble with high correspondence with the measured data. It is suggested that this upper bound could represent a natural upper limit for this rock or

fracture type, and the gradient of this trend may change depending on different rock types and stress state under which the fracture was induced. This method does not solely rely on full surface scans and can be readily used on surface profiles, in which case, the parameter inputs should be obtained preferably with a relatively short maximum step length of 5%.

The way in which the surfaces are generated and the correlation between them, up-scaling of the generated apertures can be easily achieved. When the 75^{th} percentiles for Hurst exponent and scaling parameter are calculated for a subsection of the full surfaces, the values are close to the linear regression calculated for the full surface. These values and the correlation between upper and lower surfaces of the subsection were successfully used to generate up-scaled aperture fields representing the full surface with moderately high correspondence. Aperture fields generated using this method are representative of natural fracture apertures and could be used for modelling larger fractures or multiple fractures, allowing for large scale discrete fracture network simulations to include realistic representation of aperture internal heterogeneity.

6 Data availability statement

The fracture surface data used for supporting the results presented in this paper are openly available from `https://doi.org/10.5281/zenodo.8354914` (Stock, 2023).

Acknowledgments

B. S. and A. F. gratefully acknowledge funding from the Swedish Nuclear Fuel and Waste Management Co. (SKB) and the Rock Engineering Research Foundation (BeFo).

References

Brown, S. (1987). Fluid flow through rock joints: The effect of surface roughness. *Journal of Geophysical Research: Solid Earth*. Retrieved 2020-08-31, from `https://agupubs.onlinelibrary.wiley.com/doi/abs/10.1029/JB092iB02p01337?casa_token=tRMmqdF21RoAAAAA:xztBT0RA4hXEgMe_Vx_z94i2XHXTsnCbhKnfCwChe1n7BV5zMsvcTCQN82UPQCLQTBavAW4mfiuu6DU`

Brown, S. R. (1995a). Measuring the Dimension of Self-Affine Fractals: Example of Rough Surfaces. In C. C. Barton & P. R. La Pointe (Eds.), *Fractals in the Earth Sciences* (pp. 77–87). Boston, MA: Springer US. Retrieved 2022-11-10, from `https://doi.org/10.1007/978-1-4899-1397-5_4` doi: 10.1007/978-1-4899-1397-5_4

Brown, S. R. (1995b). Simple mathematical model of a rough fracture. *Journal of Geophysical Research: Solid Earth*, *100*(B4), 5941–5952. Retrieved 2021-10-05, from `https://onlinelibrary.wiley.com/doi/abs/10.1029/94JB03262` (_eprint: https://onlinelibrary.wiley.com/doi/pdf/10.1029/94JB03262) doi: 10.1029/94JB03262

Brown, S. R. (1998). *Experimental observation of fluid flow channels in a single fracture - Brown - 1998 - Journal of Geophysical Research: Solid Earth - Wiley Online Library.* Retrieved 2020-08-31, from `https://agupubs.onlinelibrary.wiley.com/doi/abs/10.1029/97JB03542`

Brown, S. R., & Scholz, C. H. (1985). Closure of random elastic surfaces in contact. *Journal of Geophysical Research: Solid Earth*, *90*(B7), 5531–5545. Retrieved 2022-05-24, from `https://onlinelibrary.wiley.com/doi/abs/10.1029/JB090iB07p05531` (_eprint: https://onlinelibrary.wiley.com/doi/pdf/10.1029/JB090iB07p05531) doi: 10.1029/JB090iB07p05531

Bruines, P. (2022). *Description of Task 10.2 - Channelling in a single fracture.*

Task 10 of SKB Task Force GWFTS - Validation approaches for groundwater flow and transport modelling with discrete features. SKB P-22-06, Svensk Kärnbränslehantering AB.

Cacas, M. C., Ledoux, E., Marsily, G. d., Tillie, B., Barbreau, A., Durand, E., ... Peaudecerf, P. (1990). Modeling fracture flow with a stochastic discrete fracture network: calibration and validation: 1. The flow model. *Water Resources Research*, *26*(3), 479–489. Retrieved 2020-09-17, from https://agupubs.onlinelibrary.wiley.com/doi/abs/10.1029/WR026i003p00479 (_eprint: https://agupubs.onlinelibrary.wiley.com/doi/pdf/10.1029/WR026i003p00479) doi: 10.1029/WR026i003p00479

Candela, T., Renard, F., Bouchon, M., Brouste, A., Marsan, D., Schmittbuhl, J., & Voisin, C. (2009, October). Characterization of Fault Roughness at Various Scales: Implications of Three-Dimensional High Resolution Topography Measurements. *Pure and Applied Geophysics*, *166*(10-11), 1817–1851. Retrieved 2021-06-02, from http://link.springer.com/10.1007/s00024-009-0521-2 doi: 10.1007/s00024-009-0521-2

Durham, W. B., & Bonner, B. P. (1994). Self-propping and fluid flow in slightly offset joints at high effective pressures. *Journal of Geophysical Research: Solid Earth*, *99*(B5), 9391–9399. Retrieved 2020-04-24, from https://agupubs.onlinelibrary.wiley.com/doi/abs/10.1029/94JB00242 (_eprint: https://agupubs.onlinelibrary.wiley.com/doi/pdf/10.1029/94JB00242) doi: 10.1029/94JB00242

Frampton, A., & Cvetkovic, V. (2011). Numerical and analytical modeling of advective travel times in realistic three-dimensional fracture networks. *Water Resources Research*, *47*(2). Retrieved 2022-04-05, from https://onlinelibrary.wiley.com/doi/abs/10.1029/2010WR009290 (_eprint: https://onlinelibrary.wiley.com/doi/pdf/10.1029/2010WR009290) doi: 10.1029/2010WR009290

Frampton, A., Hyman, J. D., & Zou, L. (2019). Advective Transport in Discrete Fracture Networks With Connected and Disconnected Textures Representing Internal Aperture Variability. *Water Resources Research*, *55*(7), 5487–5501. Retrieved 2022-04-05, from https://onlinelibrary.wiley.com/doi/abs/10.1029/2018WR024322 (_eprint: https://onlinelibrary.wiley.com/doi/pdf/10.1029/2018WR024322) doi: 10.1029/2018WR024322

Gallant, J. C., Moore, I. D., Hutchinson, M. F., & Gessler, P. (1994, May). Estimating fractal dimension of profiles: A comparison of methods. *Mathematical Geology*, *26*(4), 455–481. Retrieved 2022-09-01, from https://doi.org/10.1007/BF02083489 doi: 10.1007/BF02083489

Glover, P. W. J., Matsuki, K., Hikima, R., & Hayashi, K. (1998a). Fluid flow in synthetic rough fractures and application to the Hachimantai geothermal hot dry rock test site. *Journal of Geophysical Research: Solid Earth*, *103*(B5), 9621–9635. Retrieved 2022-02-15, from https://onlinelibrary.wiley.com/doi/abs/10.1029/97JB01613 (_eprint: https://onlinelibrary.wiley.com/doi/pdf/10.1029/97JB01613) doi: 10.1029/97JB01613

Glover, P. W. J., Matsuki, K., Hikima, R., & Hayashi, K. (1998b). Synthetic rough fractures in rocks. *Journal of Geophysical Research: Solid Earth*, *103*(B5), 9609–9620. Retrieved 2022-11-10, from https://onlinelibrary.wiley.com/doi/abs/10.1029/97JB02836 (_eprint: https://onlinelibrary.wiley.com/doi/pdf/10.1029/97JB02836) doi: 10.1029/97JB02836

Hakami, E. (1995). *Aperture distribution of rock fractures* (Tech. Rep. Nos. KTH-AMI-PHD–1003). Royal Inst. of Tech. Retrieved 2020-07-30, from http://inis.iaea.org/Search/search.aspx?orig_q=RN:27020199

Hurst, H. E. (1951, January). Long-Term Storage Capacity of Reservoirs. *Transactions of the American Society of Civil Engineers*, *116*(1), 770–799. Retrieved 2022-09-01, from https://ascelibrary.org/doi/10.1061/TACEAT.0006518 (Publisher: American Society of Civil Engineers) doi: 10.1061/TACEAT.0006518

Isakov, E., Ogilvie, S. R., Taylor, C. W., & Glover, P. W. J. (2001, September). Fluid flow through rough fractures in rocks I: high resolution aperture determinations. *Earth and Planetary Science Letters*, *191*(3), 267–282. Retrieved 2023-01-03, from https://www.sciencedirect.com/science/article/pii/S0012821X01004241 doi: 10.1016/S0012-821X(01)00424-1

Keller, A. A., Roberts, P. V., & Blunt, M. J. (1999). Effect of fracture aperture variations on the dispersion of contaminants. *Water Resources Research*, *35*(1), 55–63. Retrieved 2023-01-03, from https://onlinelibrary.wiley.com/doi/abs/10.1029/1998WR900041 (_eprint: https://onlinelibrary.wiley.com/doi/pdf/10.1029/1998WR900041) doi: 10.1029/1998WR900041

Lang, P. S., Paluszny, A., & Zimmerman, R. W. (2014). Permeability tensor of three-dimensional fractured porous rock and a comparison to trace map predictions. *Journal of Geophysical Research: Solid Earth*, *119*(8), 6288–6307. Retrieved 2020-09-12, from https://agupubs.onlinelibrary.wiley.com/doi/abs/10.1002/2014JB011027 (_eprint: https://agupubs.onlinelibrary.wiley.com/doi/pdf/10.1002/2014JB011027) doi: 10.1002/2014JB011027

Malinverno, A. (1990). A simple method to estimate the fractal dimension of a self-affine series. *Geophysical Research Letters*, *17*(11), 1953–1956. Retrieved 2021-11-29, from https://onlinelibrary.wiley.com/doi/abs/10.1029/GL017i011p01953 (_eprint: https://onlinelibrary.wiley.com/doi/pdf/10.1029/GL017i011p01953) doi: 10.1029/GL017i011p01953

Mandelbrot, B. (1982). *The Fractal Geometry of Nature* (Vol. 1). WH Freeman New York.

Marsch, K., & Fernandez-Steeger, T. M. (2021, April). Comparative Evaluation of Statistical and Fractal Approaches for JRC Calculation Based on a Large Dataset of Natural Rock Traces. *Rock Mechanics and Rock Engineering*, *54*(4), 1897–1917. Retrieved 2021-11-24, from http://link.springer.com/10.1007/s00603-020-02348-0 doi: 10.1007/s00603-020-02348-0

Nicholl, M. J., Rajaram, H., Glass, R. J., & Detwiler, R. (1999). Saturated flow in a single fracture: evaluation of the Reynolds Equation in measured aperture fields. *Water Resources Research*, *35*(11), 3361–3373. Retrieved 2020-08-31, from https://agupubs.onlinelibrary.wiley.com/doi/abs/10.1029/1999WR900241 (_eprint: https://agupubs.onlinelibrary.wiley.com/doi/pdf/10.1029/1999WR900241) doi: 10.1029/1999WR900241

Novakowski, K. S., & Lapcevic, P. A. (1994). Field measurement of radial solute transport in fractured rock. *Water Resources Research*, *30*(1), 37–44. Retrieved 2020-08-31, from https://agupubs.onlinelibrary.wiley.com/doi/abs/10.1029/93WR02401 (_eprint: https://agupubs.onlinelibrary.wiley.com/doi/pdf/10.1029/93WR02401) doi: 10.1029/93WR02401

Ogilvie, S. R., Isakov, E., & Glover, P. W. (2006, January). Fluid flow through rough fractures in rocks. II: A new matching model for rough rock fractures. *Earth and Planetary Science Letters*, *241*(3-4), 454–465. Retrieved 2021-10-05, from https://linkinghub.elsevier.com/retrieve/pii/S0012821X05008174 doi: 10.1016/j.epsl.2005.11.041

Ogilvie, S. R., Isakov, E., Taylor, C. W., & Glover, P. W. J. (2003, January).

Characterization of rough-walled fractures in crystalline rocks. *Geological Society, London, Special Publications*, *214*(1), 125–141. Retrieved 2023-01-03, from https://www.lyellcollection.org/doi/abs/10.1144/gsl.sp.2003.214.01.08 (Publisher: The Geological Society of London) doi: 10.1144/GSL.SP.2003.214.01.08

Power, W. L., & Tullis, T. E. (1991). Euclidean and fractal models for the description of rock surface roughness. *Journal of Geophysical Research: Solid Earth*, *96*(B1), 415–424. Retrieved 2022-09-01, from https://onlinelibrary.wiley.com/doi/abs/10.1029/90JB02107 (_eprint: https://onlinelibrary.wiley.com/doi/pdf/10.1029/90JB02107) doi: 10.1029/90JB02107

Power, W. L., & Tullis, T. E. (1992). The contact between opposing fault surfaces at Dixie Valley, Nevada, and implications for fault mechanics. *Journal of Geophysical Research: Solid Earth*, *97*(B11), 15425–15435. Retrieved 2022-02-15, from https://onlinelibrary.wiley.com/doi/abs/10.1029/92JB01059 (_eprint: https://onlinelibrary.wiley.com/doi/pdf/10.1029/92JB01059) doi: 10.1029/92JB01059

Renard, F., Voisin, C., Marsan, D., & Schmittbuhl, J. (2006). High resolution 3D laser scanner measurements of a strike-slip fault quantify its morphological anisotropy at all scales. *Geophysical Research Letters*, *33*(4). Retrieved 2021-09-15, from https://onlinelibrary.wiley.com/doi/abs/10.1029/2005GL025038 (_eprint: https://agupubs.onlinelibrary.wiley.com/doi/pdf/10.1029/2005GL025038) doi: 10.1029/2005GL025038

Stigsson, M., & Mas Ivars, D. (2019, April). A Novel Conceptual Approach to Objectively Determine JRC Using Fractal Dimension and Asperity Distribution of Mapped Fracture Traces. *Rock Mechanics and Rock Engineering*, *52*(4), 1041–1054. Retrieved 2021-05-26, from http://link.springer.com/10.1007/s00603-018-1651-6 doi: 10.1007/s00603-018-1651-6

Stock, B. (2023, September). *Fracture surface data* [dataset]. Retrieved from https://doi.org/10.5281/zenodo.8354914 doi: 10.5281/zenodo.8354914

Stock, B., & Frampton, A. (2022, June). Processing and Conversion of Raw Point-Cloud Laser Measurements and Auxiliary Data of Rough-Surfaced Fractures To Generate Corresponding Fracture Aperture Fields. OnePetro. Retrieved 2023-05-16, from https://onepetro.org/ARMADFNE/proceedings-abstract/DFNE22/All-DFNE22/515893 doi: 10.56952/ARMA-DFNE-22-0020

Tsang, C.-F., & Neretnieks, I. (1998). Flow channeling in heterogeneous fractured rocks. *Reviews of Geophysics*, *36*(2), 275–298. Retrieved 2022-08-24, from https://onlinelibrary.wiley.com/doi/abs/10.1029/97RG03319 (_eprint: https://onlinelibrary.wiley.com/doi/pdf/10.1029/97RG03319) doi: 10.1029/97RG03319

Witherspoon, P. A., Wang, J. S. Y., Iwai, K., & Gale, J. E. (1980). Validity of Cubic Law for fluid flow in a deformable rock fracture. *Water Resources Research*, *16*(6), 1016–1024. Retrieved 2020-07-21, from https://agupubs.onlinelibrary.wiley.com/doi/abs/10.1029/WR016i006p01016 (_eprint: https://agupubs.onlinelibrary.wiley.com/doi/pdf/10.1029/WR016i006p01016) doi: 10.1029/WR016i006p01016

Zimmerman, R. W., & Bodvarsson, G. S. (1996, April). Hydraulic conductivity of rock fractures. *Transport in Porous Media*, *23*(1), 1–30. Retrieved 2019-11-11, from https://doi.org/10.1007/BF00145263 doi: 10.1007/BF00145263

Zou, L., Jing, L., & Cvetkovic, V. (2017, September). Modeling of flow and mixing in 3D rough-walled rock fracture intersections. *Advances in Water Resources*, *107*, 1–9. Retrieved 2021-06-14, from https://www.sciencedirect.com/science/article/pii/S0309170816305097 doi: 10.1016/j.advwatres.2017.06.003